Journal of Power Sources 189 (2009) 882–887

Contents lists available at ScienceDirect

Journal of Power Sources

journal homepage: www.elsevier.com/locate/jpowsour

Experimental research on water management in proton exchange membrane fuel cells

Li-jun Yu [a,*], Wen-can Chen [a], Ming-jun Qin [a], Geng-po Ren [b]

[a] Institute of Thermal Energy Engineering, School of Mechanical Engineering, Shanghai Jiao Tong University, Shanghai 200240, China
[b] Shanghai Energy Conservation Supervision Center, Shanghai 200011, China

ARTICLE INFO

Article history:
Received 16 November 2008
Received in revised form 16 January 2009
Accepted 16 January 2009
Available online 24 February 2009

Keywords:
Proton exchange membrane (PEM) fuel cell
Gas–liquid two-phase flow
Flow regime
Double parallel conductance probes

ABSTRACT

A simulated cathode flow channel experiment system was set up based on the gas flow rate and water flow rate in the PEM fuel cell. With the assistance of the visualization system, high-sensitivity double parallel conductance probes flow regime inspecting technique was adopted successfully in the experiment system to inspect the flow regime of the gas–liquid two-phase flow in the PEM fuel cell. The research results show that the double parallel conductance probes inspecting system and the flow regime image system for the gas–liquid two-phase flow in the PEM fuel cell simulated channel both can judge the slug flow and annular flow in it, and the double parallel conductance probes flow regime inspecting system can divide the annular flow into three subtypes. The main probes inspecting system and the assistant image system validate reciprocally, which enhances the experimental veracity. The typical flow regimes of the PEM fuel cell simulated channel include slug flow, annular flow with big water film wave, annular flow with small water film wave and annular flow without water film wave. With the increase of the liquid superficial velocity, the frequencies of liquid slug and wave of liquid film increase. The flow regime map in the flow channel of the PEM fuel cell was developed. The flow regime of the gas–liquid two-phase flow in a PEM fuel cell in different operating conditions can be forecasted with this map. With the PEM fuel cell operating condition in this study, the flow regimes of gas–liquid two-phase flow for different cases are all annular flow with small water film wave, and the liquid film waves more with bigger current density. With the location closer to the channel outlet, the liquid film waves are more for the same current density.

1. Introduction

One of the main characteristics of a proton exchange membrane (PEM) fuel cell is the liquid status of cathode electrochemical reaction production. When the current density reaches a relatively high value, the gas–liquid two-phase flow in the PEM fuel cell comes out [1]. Liquid water floods the cathode, which will reduce the gas utilization ratio and the effective area of the catalyst layer. When the PEM fuel cell works at high current density, the mass transfer, related to water generation and distribution, restrict the fuel cell performance [2].

The main purpose of water management is to prevent the mentioned cathode flood, so as to keep the proper water content in the membrane and to remove the liquid water in the cathode flow channel of the PEM fuel cell. As a result, the performance of the PEM fuel cell will be improved.

Gas–liquid two-phase flow is a common phenomenon in the operation of the low-temperature PEM fuel cell. Previous studies have focused on two dimensions of the fuel cell: one direction parallel to membrane in the direction of bulk flow and the other direction across the membrane. Many researchers have researched the liquid–gas two-phase flow of PEMFC [3–12]. Y. Zhang and C. Zhu developed the flow models, and made a lot description on it. I.M. Hsing demonstrated the phenomenon of different flow regimes and different conditions.

In this experiment a simulated cathode flow channel experiment system was set up based on the gas flow rate and water flow rate in the PEM fuel cell. With the assistance of the visualization system, high-sensitivity double parallel conductance probes flow regime inspecting technique [13] was adopted successfully in the experiment system to inspect the flow regime of the gas–liquid two-phase flow in the PEM fuel cell. The probe inspecting system can research the cell unit that is not located by the cathode end-plate. The main probes inspecting system and the assistant image system validate reciprocally, which enhances the experimental veracity.

* Corresponding author. Tel.: +86 21 3420 6287; fax: +86 21 3420 6287.
E-mail address: ljyu@sjtu.edu.cn (L.-j. Yu).

0378-7753/$ – see front matter © 2009 Elsevier B.V. All rights reserved.
doi:10.1016/j.jpowsour.2009.01.037

Nomenclature

d	channel width (m)
F	Faraday constant (96485 C mol^{-1})
h	channel depth (m)
I_{avg}	average current density (Am^{-2})
j_G	air superficial velocity (ms^{-1})
j_L	water superficial velocity (ms^{-1})
l	channel length (m)
l_{out}	distance between the test position and channel outlet (m)
n	peristaltic pump rotation speed (rpm)
V_G	air flow rate (sccm)
V_L	water flow rate (ml min^{-1})
w	channel rib width (m)

Subscripts

con	consumption
e	test
ele	electrochemistry
trans	transfer
in	channel inlet

Greece letters

α	net water flux per proton flux
β	air stoichiometric ratio
ρ_l	density of the water

2. Experimental assembly

2.1. Gas and water supply system

Figs. 1 and 2 show the gas and water supply system, and the system includes air cylinder, pressure-relief valve, mass flow controller and flow indicating instrument, peristaltic pump, and PEM fuel cell simulated flow channel. Air cylinder provided clean experimental gas, which was also the need of mass flow controller. Pressure-relief valve relieved the air pressure to the working pressure range of the mass flow controller (0.1–0.5 MPa). Mass flow controller and flow indicating instrument controlled and indicated the air flow rate into the simulated flow channel. Peristaltic pump controlled the water flow rate into the simulated flow channel.

Fig. 3 shows the PEM fuel cell simulated flow channel which was made of plexiglass. The size of the flow channel is 50 mm × 1 mm × 1 mm. Air and water entered the PEM fuel cell simulated flow channel through the gas and liquid inlets separately. The probes hole was utilized to dispose the double parallel conductance probes.

Table 1
Basic data for the calculation of the experimental cases design.

Parameters	Values
Channel length (l)	5.0×10^{-2} m
Channel depth (h)	1.0×10^{-3} m
Channel width (d)	1.0×10^{-3} m
Channel rib width (w)	1.0×10^{-3} m
Air superficial velocity in channel inlet ($j_{G,in}$)	1.0 ms^{-1}

2.2. Conductance probes testing system and visualization photography system

Conductance probes testing system and visualization photography system of the experiment showed in Figs. 1 and 2 include double parallel conductance probes, regulated power supply, actuating signal generator, probes signal conditioning circuit, data collecting card, camera head, personal computer, and light source.

(1) Double parallel conductance probes
Two platinum filaments whose diameter was 0.05 mm were chosen as the double parallel conductance probes, and the gap between them was 1 mm.
(2) Regulated power supply
Regulated power supply supplied direct current voltage for the probes signal conditioning circuit.
(3) Actuating signal generator
Actuating signal generator provided sine actuating signal for the probes signal conditioning circuit.
(4) Probes signal conditioning circuit

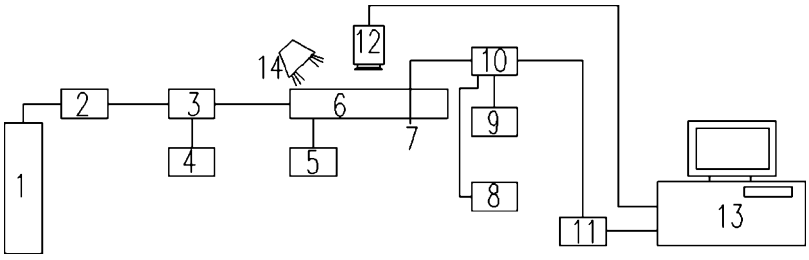

Fig. 1. Experimental theory for the gas–liquid two-phase flow in the PEMFC. (1) air cylinder, (2) pressure-relief valve, (3) mass flow controller, (4) flow indicating instrument, (5) peristaltic pump, (6) PEM fuel cell simulated flow channel, (7) double parallel conductance probes, (8) regulated power supply, (9) actuating signal generator, (10) probes signal conditioning circuit, (11) data collecting card, (12) camera head, (13) personal computer, (14) light source.

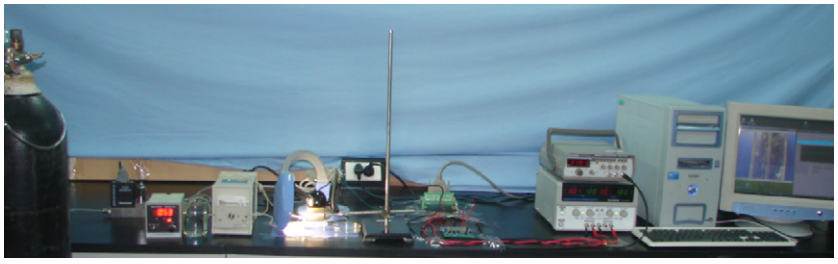

Fig. 2. Experimental facility for the gas–liquid two-phase flow in the PEMFC.

Table 2
Calculation results of the experimental cases for the flow regime map.

Air superficial velocity j_G (ms^{-1})	Air flow rate V_G (sccm)	Water superficial velocity j_L (ms^{-1})	Water flow rate V_L ($ml\,min^{-1}$)	Pump rotation speed n (rpm)
0.01	0.6	0.0002	0.012	1.0
0.02	1.2	0.0004	0.024	1.9
0.04	2.4	0.0008	0.048	3.8
0.08	4.8	0.002	0.12	9.5
0.14	8.4	0.004	0.24	19.0
0.2	12	0.008	0.48	38
0.4	24	0.014	0.84	66
0.8	48	0.02	1.2	95
1.4	84			
2	120			
3.2	192			

Probes signal conditioning circuit inverted the double parallel conductance probes signal into collectable voltage signal.

(5) Data collecting card
Data collecting card collected the double parallel conductance probes signal with a self-programmed LabVIEW8.2 collecting program.

(6) Camera head
Camera head took photographs of gas–liquid two-phase flow in the PEM fuel cell simulated flow channel.

(7) Personal computer
Personal computer supplied support for the double parallel conductance probes signal collection and photographs signal collection.

3. Experimental project and cases

3.1. Experimental project

In order to perform the study of the PEM fuel cell gas–liquid two-phase flow, an experiment system showed in Figs. 1 and 2 was set up in School of Mechanical Engineering, Shanghai Jiao Tong University. Air was supplied and its superficial velocity in the PEM fuel cell simulated flow channel was controlled through air cylinder, pressure-relief valve and mass flow controller in order. Water was supplied and its superficial velocity in the PEM fuel cell simulated flow channel was controlled through the peristaltic pump. The gas–liquid two-phase flow flowed into a collecting container. The flow regime of the gas–liquid two-phase flow in the PEM fuel cell simulated flow channel was determined by the double parallel conductance probes signal and photographs signal. The flow channel is made of hydrophilic plexiglass. This is the same as the situation of PEMFC which uses the carbon plates or metal plates. The experiment result of the simulation flow channel can reflect the real situation of the PEMFC.

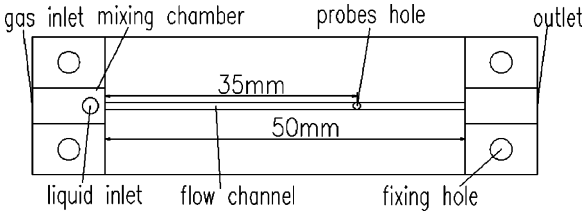

Fig. 3. Simulated flow channel for the PEMFC.

The experimental parameters covered in this experiment are as follows: the air superficial velocity $j_G = 0.01–3.2\ ms^{-1}$, while the water superficial velocity $j_L = 0.0002–0.02\ ms^{-1}$. Experiments were carried out under atmospheric pressure condition (0.1 MPa) and at room temperature (22 °C).

3.2. Experimental cases calculation

3.2.1. Calculation model

The air flow rate in the PEM fuel cell simulated flow channel is calculated by:

$$V_G = j_G\, dh \tag{1}$$

where V_G is air flow rate; j_G is air superficial velocity; d is flow channel width; h is flow channel depth.

The water flow rate in the PEM fuel cell simulated flow channel is calculated by:

$$V_L = j_L\, dh \tag{2}$$

where V_L is water flow rate; j_L is water superficial velocity.

Based on the relationship between water flow rate and pump rotation speed, the pump rotation speed can be calculated by:

$$n = \frac{V_L}{0.01262} \tag{3}$$

where n is the pump rotation speed.

The air flow rate and water flow rate calculating process for a working PEM fuel cell is as following.

The inlet air flow rate is calculated by:

$$V_{G,in} = j_{G,in}\, dh \tag{4}$$

where the subscript "in" is flow channel inlet.

Table 3
Calculation results of the experimental cases for the PEMFC in operation.

Distance from channel outlet l_{out} (mm)	Average current density I_{avg} (Am^{-2})	Air superficial velocity $j_{G,e}$ (ms^{-1})	Air flow rate $V_{G,e}$ (sccm)	Water superficial velocity $j_{L,e}$ (ms^{-1})	Water flow rate $V_{L,e}$ ($ml\,min^{-1}$)	Pump rotation speed n (rpm)	Net water transport coefficient
0	2000	0.985	59.1	0.000209	0.0125	1.0	0.61835
	6000	0.955	57.3	0.000517	0.0310	2.5	0.42352
	10000	0.925	55.5	0.000802	0.0481	3.9	0.35996
	14000	0.895	53.7	0.001100	0.0658	5.3	0.33946
10	10000	0.940	56.4	0.000642	0.0385	3.1	0.35996
20	10000	0.955	57.3	0.000481	0.0289	2.3	0.35996
30	10000	0.970	58.2	0.000321	0.0193	1.5	0.35996

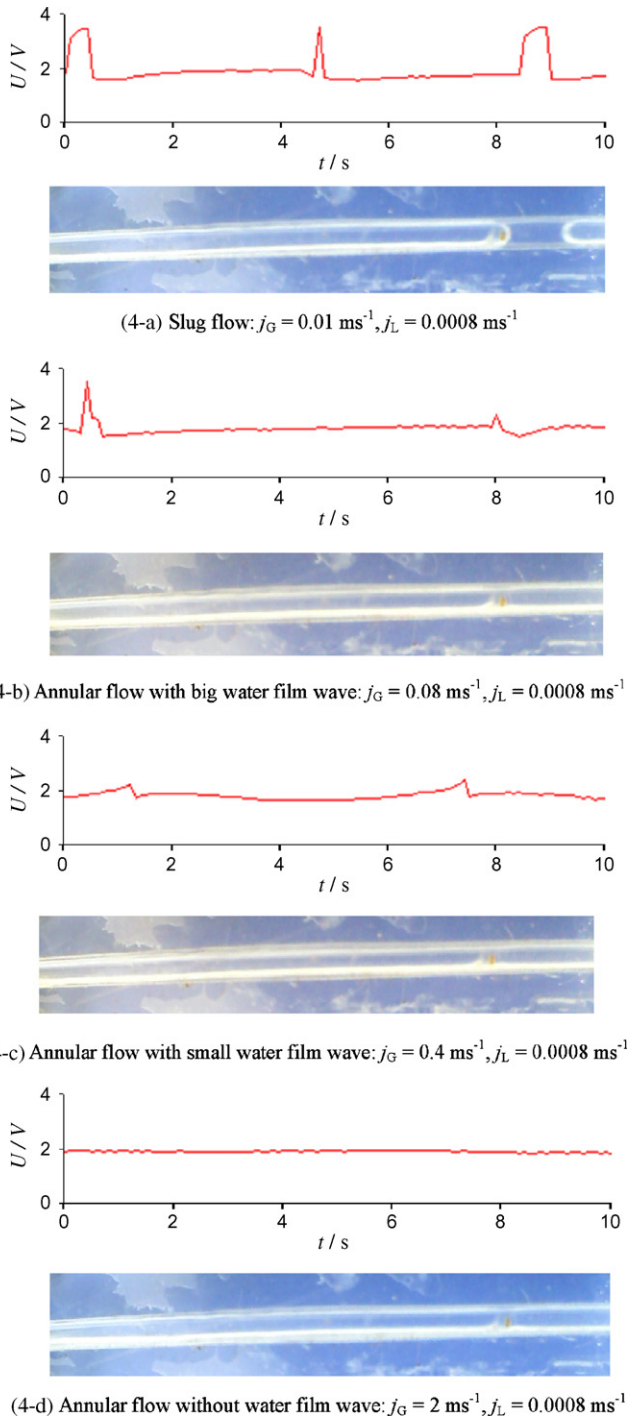

Fig. 4. Representative flow patterns in the simulated flow channel and probes voltage signals. (a) Slug flow: $j_G = 0.01$ ms^{-1}, $j_L = 0.0008$ ms^{-1}. (b) Annular flow with big water film wave: $j_G = 0.08$ ms^{-1}, $j_L = 0.0008$ ms^{-1}. (c) Annular flow with small water film wave: $j_G = 0.4$ ms^{-1}, $j_L = 0.0008$ ms^{-1}. (d) Annular flow without water film wave: $j_G = 2$ ms^{-1}, $j_L = 0.0008$ ms^{-1}.

Based on the definition formula of electric current, there is a relationship for a single PEM fuel cell flow channel.

$$I_{avg} \times (w + d) \times l = \frac{0.21 \times V_{G,in} \times (273/273 + 80)}{\beta \times 22400 \times 60} \times 4F \quad (5)$$

where I_{avg} is average current density; w is flow channel rib width; l is flow channel length; β is air stoichiometric ratio; F is Faraday constant. The air stoichiometric ratio was assumed as 2.0.

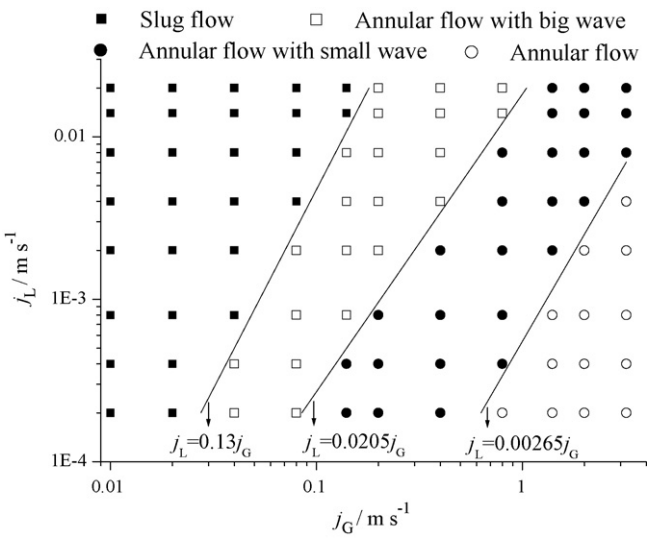

Fig. 5. Flow regime map for the simulated flow channel.

The consumption oxygen flow rate at the test position is calculated by:

$$V_{G,con} = \frac{l - l_{out}}{l} 0.21 \times \frac{V_{G,in}}{\beta} \quad (6)$$

where the subscript "con" is consumption; l_{out} is the distance between the test position and flow channel outlet. For simplification, we assume that the current density is equal along the flow channel.

The gas flow rate at the test position is calculated by:

$$V_{G,e} = V_{G,in} - V_{G,con} \quad (7)$$

where the subscript "e" is test.

The water flow rate for the production of the electrochemistry reaction in the PEM fuel cell is calculated by:

$$V_{L,e,ele} = \frac{V_{G,con}}{22,400} \times 2 \times 18 \times \frac{273}{273 + 80} \times \frac{1}{\rho_l} \quad (8)$$

where the subscript "ele" is electrochemistry, ρ_l is the density of water.

In fluorinated membranes (e.g., Nafion), water is transported by electroosmotic drag, back diffusion, and permeation. [14,15]. In this simulated flow channel of PEMFC, we assumed anode and cathode pressures are equal. The accumulative net water flow rate through the membrane ($V_{L,e,trans}$, m^3 s^{-1}) can thus be written as:

$$V_{L,e,trans} = \alpha \times \frac{V_{G,con}}{22,400} \times 4 \times 18 \times \frac{273}{273+80} \times \frac{1}{\rho_l} \quad (9)$$

where the subscript "trans" is transfer; α is the net water transfer coefficient.

In order to simplify the subsystem of PEMFC stacks, the operation of PEMFCs without external humidification of the reactant gases is advantageous [16,17]. In the simulated flow channel of PEMFC, we do not consider air humidification. So water comes from electrochemical reaction and net water transport. The water rate in the testing position is:

$$V_{L,e} = V_{L,e,ele} + V_{L,e,trans} \quad (10)$$

3.2.2. Calculation results

Table 1 shows the basic data for the calculation of the experimental cases design. The air flow rate, the water flow rate and the pump rotation speed are calculated at the ranges of air superficial velocity $j_G = 0.01$–3.2 ms^{-1} and water superficial velocity

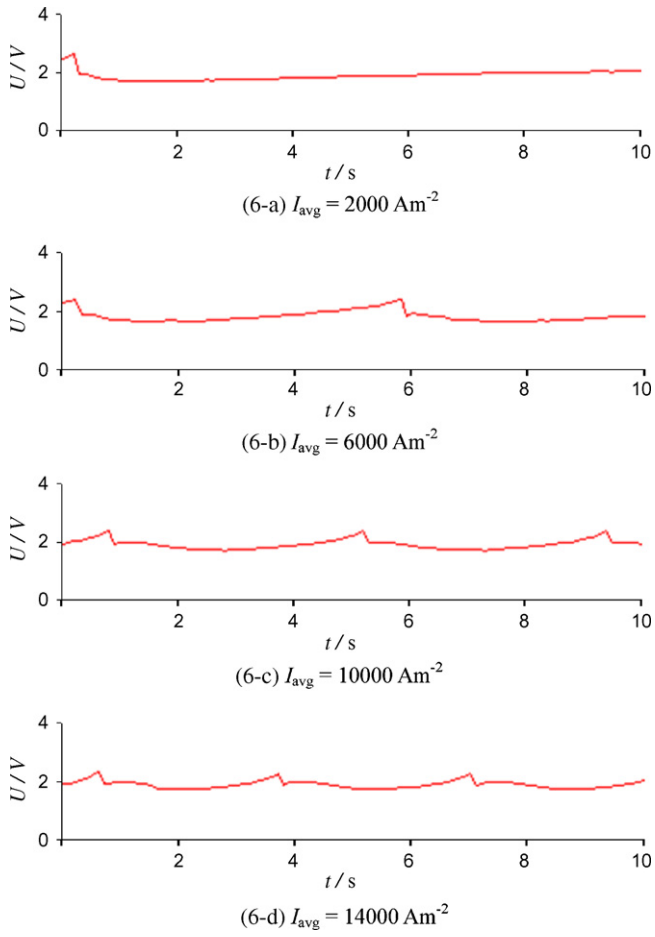

Fig. 6. Probes voltage signals for the simulated flow channel outlet with different current density. (a) I_{avg} = 2000 Am^{-2}. (b) I_{avg} = 6000 Am^{-2}. (c) I_{avg} = 10000 Am^{-2}. (d) I_{avg} = 14000 Am^{-2}.

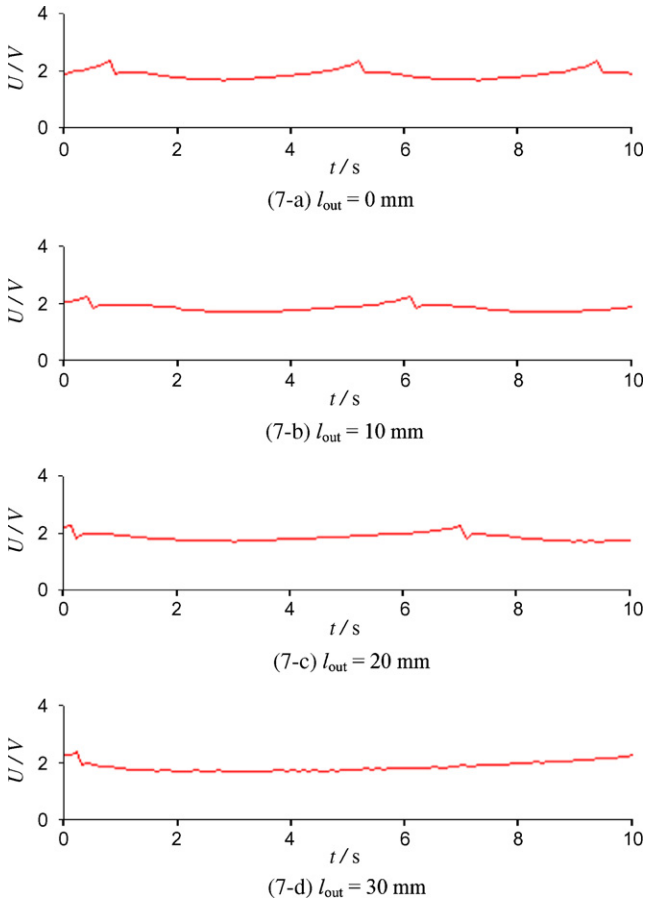

Fig. 7. Probes voltage signals for the simulated flow channel at different location for I_{avg} = 10000 Am^{-2}. (a) l_{out} = 0 mm. (b) l_{out} = 10 mm (c) l_{out} = 20 mm. (d) l_{out} = 30 mm.

j_L = 0.0002–0.02 ms^{-1}, and Table 2 shows the calculation results. The air superficial velocity, the air flow rate, the water superficial velocity, the water flow rate and the pump rotation speed are calculated for different average current density and different testing positions, and Table 3 shows the calculation results.

4. Experimental results

4.1. Representative flow regimes

Fig. 4 shows the representative flow regimes in the simulated flow channel and probes voltage signals. The slug flow (Fig. 4(a)) appears at small air superficial velocity. The water slug and the air slug are corresponding to big and small voltage signals of the probes, respectively. With the increase of the air superficial velocity, the annular flow with big water film wave (Fig. 4(b)) appears. The flow channel was surrounded by waving water film. When a waving water film flows through the probes, a voltage impulse of the probes appears. With the further increase of the air superficial velocity, the water film waving extant decreases, and the annular flow with small water film wave (Fig. 4(c)) appears. The relatively smaller waving water film induces the relatively smaller voltage impulse of the probes. With the further increase of the air superficial velocity, the annular flow without water film wave (Fig. 4(d)) appears.

It is known from the above analysis that the double parallel conductance probes inspecting system and the flow regime image system for the gas–liquid two-phase flow in the PEM fuel cell simulated channel both can judge the slug flow and annular flow in it, and the former can further divide the annular flow into three subtypes. The main probes inspecting system and the assistant image system validate reciprocally, which enhances the experimental veracity.

4.2. Flow regime map

The experiment was performed according to the cases showed in Table 2. The gas–liquid two-phase flow in the PEM fuel cell simulated channel was judged both with the double parallel conductance probes signals and the flow regime image signals. Fig. 5 shows the flow regime map for the simulated flow channel. It is known from the figure that, at the fixed water superficial velocity, the slug flow, the annular flow with big water film wave, the annular flow with small water film wave and the annular flow without water film wave appear in turn with the increase of the air superficial velocity.

4.3. Flow regimes for the simulated flow channel with different operating conditions

The experiment was performed according to the cases showed in Table 3. The effects of the average current density and the testing position on the gas–liquid two-phase flow in the PEM fuel cell simulated channel were studied. The flow regimes of the gas–liquid two-phase flow in the PEM fuel cell simulated channel with the cases in Table 3 were all the annular flow with small water film wave, and the image signals were similar to the signal in Fig. 4(c), so, the image signals in this part were not listed out.

Fig. 6 shows the probes voltage signals for the simulated flow channel outlet with different current density. The frequency of the water film wave increases with the increase of the average current density. The reason is the water production because of the electrochemical reaction in the cathode and the transferred water from the anode to the cathode both increase with the increase of the average current density.

Fig. 7 shows the probes voltage signals for the simulated flow channel at different location for the average current density $I_{avg} = 10000\,Am^{-2}$. The frequency of the water film wave increases with the testing position closer to the channel outlet. The reason is the water production because of the electrochemical reaction in the cathode, the transferred water from the anode to the cathode, and the oxygen consumption proceed step by step along the channel.

5. Conclusions and discussion

A simulated cathode flow channel experiment system was set up based on the gas flow rate and the water flow rate in the PEM fuel cell. With the assistant of the visualization system, high-sensitivity double parallel conductance probes flow regime inspecting technique was adopted successfully in the experiment system to inspect the flow regime of the gas–liquid two-phase flow in the PEM fuel cell. Based on the analysis on the experiment results, the main conclusions were obtained:

(1) The double parallel conductance probes inspecting system and the flow regime image system for the gas–liquid two-phase flow in the PEM fuel cell simulated channel both can judge the slug flow and annular flow in it, and the former can further divide the annular flow into three subtypes.
(2) The representative flow regimes in the simulated flow channel include the slug flow, the annular flow with big water film wave, the annular flow with small water film wave and the annular flow without water film wave. The frequencies of the water slugs and the water film waves increase with the increase of the water superficial velocity.
(3) At the fixed water superficial velocity, the slug flow, the annular flow with big water film wave, the annular flow with small water film wave and the annular flow without water film wave appear in turn with the increase of the air superficial velocity.
(4) The flow regimes of the gas–liquid two-phase flow in the PEM fuel cell simulated channel with the cases for the operating PEM fuel cell were all the annular flow with small water film wave. The frequency of the water film wave increases with the increase of the average current density or with the testing position closer to the channel outlet.

Acknowledgements

This project was financially supported by National Natural Science Foundation of China (no.50676058), and by National 863 Plans of China (Contracts 2008AA09Z313).

References

[1] Z.H. Wang, C.Y. Wang, K.S. Chen, Journal of Power Sources 94 (1) (2001) 40–50.
[2] L. You, H. Liu, International Journal of Heat and Mass Transfer 45 (11) (2002) 2277–2287.
[3] K. Tüber, D. Pócza, C. Hebling, Journal of Power Sources 124 (2) (2003) 403–414.
[4] N. Pekula, K. Heller, P.A. Chuang, A. Turhan, M.M. Mench, J.S. Brenizer, K. Unlu, Nuclear Instruments and Methods in Physics Research A 542 (1–3) (2005) 134–141.
[5] K. Sugiura, M. Nakata, T. Yodo, Y. Nishiguchi, M. Yamauchi, Y. Itoh, Journal of Power Sources 145 (2) (2005) 526–533.
[6] F. Barreras, A. Lozano, L. Valino, C. Marin, A. Pascau, Journal of Power Sources 144 (1) (2005) 54–66.
[7] H.P. Ma, H.M. Zhang, J. Hu, Y.H. Cai, B.L. Yi, Journal of Power Sources 162 (1) (2006) 469–473.
[8] X. Liu, H. Guo, C. Ma, Journal of Power Sources 156 (2) (2006) 267–280.
[9] J.P. Owejan, T.A. Trabold, D.L. Jacobson, D.R. Baker, D.S. Hussey, International Journal of Heat and Mass Transfer 49 (25–26) (2006) 4721–4731.
[10] T. Ous, C. Arcoumanis, Journal of Power Sources 173 (1) (2007) 137–148.
[11] S. Ge, C.Y. Wang, Electrochimica Acta 52 (14) (2007) 4825–4835.
[12] X. Liu, H. Guo, F. Ye, C.F. Ma, Electrochimica Acta 52 (11) (2007) 3607–3614.
[13] M.W.E. Coney, Journal of Physics E Scientific Instruments 6 (4) (1973) 903–910.
[14] S.H. Ge, B.L. Yi, Journal of Power Sources 124 (2003) 1–11.
[15] C.Y. Wang, Chemical Reviews 104 (2004) 4727–4765.
[16] F.N. Buchi, S. Srinivasan, Journal of the Electrochemical Society 144 (1997) 2767–2772.
[17] S.H. Ge, X.G. Li, I.M. Hsing, Journal of the Electrochemical Society 151 (2004) B523–B528.